Comput Mech
DOI 10.1007/s00466-014-1044-y

ORIGINAL PAPER

Multi-physics computational grains (MPCGs) for direct numerical simulation (DNS) of piezoelectric composite/porous materials and structures

Peter L. Bishay · Leiting Dong · Satya N. Atluri

Received: 23 October 2013 / Accepted: 26 May 2014

Abstract Conceptually simple and computationally most efficient polygonal computational grains with voids/inclusions are proposed for the direct numerical simulation of the micromechanics of piezoelectric composite/porous materials with non-symmetrical arrangement of voids/inclusions. These are named "Multi-Physics Computational Grains" (MPCGs) because each "mathematical grain" is geometrically similar to the irregular shapes of the physical grains of the material in the micro-scale. So each MPCG element represents a grain of the matrix of the composite and can include a pore or an inclusion. MPCG is based on assuming independent displacements and electric-potentials in each cell. The trial solutions in each MPCG do not need to satisfy the governing differential equations, however, they are still complete, and can efficiently model concentration of electric and mechanical fields. MPCG can be used to model any generally anisotropic material as well as nonlinear problems. The essential idea can also be easily applied to accurately solve other multi-physical problems, such as complex thermal-electro-magnetic-mechanical materials modeling. Several examples are presented to show the capabilities of the proposed MPCGs and their accuracy.

Keywords Computational grains · Direct numerical simulations · Piezoelectric · Composite · Porous

P. L. Bishay · S. N. Atluri
Center for Aerospace Research and Education (CARE),
University of California, Irvine, Irvine, CA, USA

P. L. Bishay
The Hal and Inge Marcus School of Engineering,
Saint Martin's University, Lacey, WA, USA

L. Dong (✉)
Department of Engineering Mechanics, Hohai University,
Nanjing, China
e-mail: dong.leiting@gmail.com

S. N. Atluri
King Abdulaziz University,
Jeddah, Saudi Arabia

1 Introduction

Piezoelectric materials, together with the corresponding sensing and actuating devices, which are featured with the coupled electromechanical behaviors, have experienced continuously growing applications within manufacturing, automotive and aerospace engineering, medical instruments, information and telecommunication, among many other civil and military industries. In a market report by Acmite Market Intelligence [1] in 2010, the global demand on piezoelectric devices was valued at approximately *US$14.8* billion in 2010, and has been healthily increasing even in the global economic downturns.

Monolithic piezoelectric ceramics and piezoelectric polymers have their own limitations, such as high brittleness, low strength, high weight, undesirable acoustic impedance, etc. Piezoelectric composites have therefore been studied and developed in the past two decades, by exploring the advantageous behaviors of both functional piezoelectric materials and load-bearing materials such as ceramics, polymers, metals, etc. Light-weight, easily-shaped, and relatively strong piezoelectric composites have found promising applications in various sensors, actuators, and other smart devices. Therefore, a thorough understanding of the global and local behaviors of piezoelectric materials and devices, from both top–down and bottom–up approaches has great practical values and has attracted much interest from many scholars.

One of the most basic problems is to determine the electromechanical properties of the composite material, given the geometry, distribution, volume fraction and electromechanical properties of each constituent material. Besides experimental methods, semi-analytical methods have been developed in the past two decades to predict the effective material coefficients, such as: piezoelectric Hashin–Shtrikman type of bounds [2], and dilute, self-consistent, Mori–Tanaka, Green's functions methods [3–6], based on an Eshelby type of solution in an infinite medium. Several studies have also applied simple finite element models (FEM) to study the behavior of a unit-cell of piezoelectric composite in order to predict the overall material coefficients, see [7–11].

It is also of great interest to understand the local behavior of piezoelectric composite materials and structures. On one hand, stress concentration in the local scale is one possible major factor that can cause damage of the material, especially for the brittle piezoelectric constituents which are mostly used as fibers or particles buried in polymer matrices. On the other hand, the local stress and electric-displacement fields have direct effects on the performance of various multi-functional smart devices. Among a few studies, Kim et al. [12] studied the multi-scale response of smart sandwich composites and the monitoring capabilities of piezoceramic wafers. Cook and Vel [13] developed a multi-scale model to study the macro-scale and micro-scale fields of laminate plates with piezoelectric composite actuators. Keip and Schröder [14,15] developed a two-scale homogenization approach and implemented it into a so-called FE2—method which allows for the computation of macroscopic boundary value problems in consideration of microscopic representative volume elements.

All the aforementioned methods are mostly oversimplified, and difficult to implement. For example, semi-analytical methods use Eshelby type of solution in an infinite domain, and cannot account for complex topology of microstructure. It is also very difficult for semi-analytical methods to study the local mechanical and electric fields. On the other hand, although simple FEM can model both the global as well as the local behaviors of composite materials and structures, it is very inefficient and requires significantly large times and resources for computing as well as human-labor in generating a complex mesh. For this reason, most simple FEM analyses in the literature use a simple unit-cell with only one inclusion, which oversimplifies the complicated material microstructure.

For pure structural applications, an efficient and highly accurate tool for modeling the micromechanical behaviors of porous and composite materials was developed by Dong and Atluri [16–18] named as Trefftz Computational Grains (TCGs). Trefftz Computational Grains are featured with a complete Trefftz trial displacement field in each grain (which satisfies the governing differential equations a-priori), and a polynomial trial function on the grain boundaries. Because of the complete Trefftz trial functions, TCGs can not only accurately compute the overall stiffness and strength of the material, but can also easily compute the local stress/strain concentrations. The human labor of generating a compatible very fine FEM mesh is also saved, because each TCG can represent a grain of the material in the most natural way.

For some special cases of coupled electromechanical problems, the complete Trefftz trial functions can still be found. Bishay and Atluri presented Trefftz-Lekhnitsakii Grains (TLGs) [19] and Multi-region Trefftz Collocation Grains (MTCGs) [20] for modeling porous and composite piezoelectric materials using Lekhnitskii's formulation. Another example is the complicated general solution of transversely isotropic piezoelectricity, see [21] for details. However, for general anisotropic electro-mechanical problems, finding a complete Trefftz trial function, under the condition of possible body force and charges, initial strains and electric-fields, as well as inertia, will be very difficult, if not impossible. In this study, multi-physics computational grains (MPCGs) are proposed to model the micromechanics of piezoelectric composites. Similar to TCGs developed in [16–19], an MPCG element represents a grain of the composite as in Fig. 1, which can include a matrix material, an inclusion material or a pore. Independent displacements and electric potentials are also assumed in each grain. Quite differently from TCGs, the trial solutions in each MPCG do not need to satisfy the governing differential equations. However, the trial solutions in each MPCG are still complete, and can efficiently model concentration of electric and mechanical fields. MPCGs are conceptually simpler than TCGs, and can be used to model any generally anisotropic as well as nonlinear problems. The nonlinear switching phenomena in ferroelectric materials were modeled by Bishay and Atluri [22] using 2D and 3D multi-physics computational grains based on radial-basis-functions (RBFs). These switching phenomena in grains with embedded inclusions or voids will be addressed by the authors in a future study. The essential idea of MPCGs can also be easily applied to accurately solve other multi-physical problems, such as complex thermal-electro-magneto-mechanical material modeling.

The paper is organized as follows: the proposed theoretical and algorithmic formulation of MPCGs is presented in Sects. 2 and 3, numerical results are given in Sect. 4 and a summary is given in Sect. 5.

2 New hybrid variational principle for heterogeneous piezoelectricity

Consider a solid piezoelectric body Ω undergoing infinitesimal deformation. Cartesian coordinates x_i identify material particles in the solid. $\sigma_{ij}, \varepsilon_{ij}, u_i$ are components of stress

tensor, strain tensor and displacement vector respectively. D_i, E_i, φ represent electric displacement, electric field and electric potential respectively. $\bar{b}_i$ and $\bar{Q}$ represent body force and electric charge density in Ω. We use $(\,)_{,i}$ to denote partial differentiation with respect to x_i. We consider linearized electromechanical constitutive equations:

$$\begin{cases} \sigma_{ij} = \frac{\partial H}{\partial \varepsilon_{ij}} \\ D_i = \frac{\partial H}{\partial(-E_i)} \end{cases} \tag{1}$$

with the enthalpy defined as:

$$H\left(\varepsilon_{ij}, -E_i\right) = \frac{1}{2} C_{ijkl}\varepsilon_{ij}\varepsilon_{kl} - \frac{1}{2} h_{ij} E_i E_j - e_{kij} E_k \varepsilon_{ij} \tag{2}$$

Thus the governing differential equations can be expressed in terms of the primitive variables u_i and φ:

$$\left[\frac{\partial H}{\partial u_{(i,j)}}\right]_{,i} + \bar{b}_j = 0 \text{ in } \Omega \tag{3}$$

$$\left[\frac{\partial H}{\partial \varphi_{,i}}\right]_{,i} + \bar{Q} = 0 \text{ in } \Omega \tag{4}$$

where the relations $\varepsilon_{ij} = u_{(i,j)} = \frac{1}{2}(u_{i,j} + u_{j,i})$ and $-E_i = \varphi_{,i}$ were used.

The electromechanical constitutive equation can be written as:

$$\begin{aligned} \sigma_{ij} &= C_{ijkl}\varepsilon_{kl} - e_{kij} E_k \\ D_i &= e_{ikl}\varepsilon_{kl} + h_{ik} E_k \end{aligned} \tag{5}$$

or in matrix and vector notation as:

$$\begin{Bmatrix} \boldsymbol{\sigma} \\ \mathbf{D} \end{Bmatrix} = \begin{bmatrix} \mathbf{C} & -\mathbf{e}^T \\ \mathbf{e} & \mathbf{h} \end{bmatrix} \begin{Bmatrix} \boldsymbol{\varepsilon} \\ \mathbf{E} \end{Bmatrix} \text{ or } \underline{\boldsymbol{\sigma}} = \underline{\mathbf{C}}\,\underline{\boldsymbol{\varepsilon}} \tag{6}$$

where $\mathbf{C}$, $\mathbf{e}$ and $\mathbf{h}$ are the material stiffness tensor written in matrix form, piezoelectric tensor written in matrix form, and dielectric matrix respectively. The underline denotes electromechanical (combined mechanical and electrical) fields or matrices.

We further use $\bar{u}_i$, $\bar{t}_i$ to denote the prescribed displacement at S_u and the prescribed traction at S_t, respectively. We use $\bar{\varphi}$, $\bar{\omega}$ to denote the prescribed electric potential at S_φ and the prescribed surface charge density at S_ω. Moreover, we consider that the domain Ω is discretized into subdomains (or grains) Ω^e so that $\Omega = \sum_e \Omega^e$. The division of the boundary of grain e, $\partial\Omega^e$, according to the boundary conditions leads to $\partial\Omega^e = S_u^e + S_t^e + \rho^e = S_\varphi^e + S_\omega^e + \rho^e$, where ρ^e represents the interfaces of subdomains.

Primitive field variational principle, corresponding to the stationary condition of the following functional, is generally used to develop primal FEMs:

$$\begin{aligned} \pi_p\left(u_i, \varphi\right) &= \sum_e \pi_p^e, \\ \pi_p^e &= \int_{\Omega^e} \left[H\left(u_{(i,j)}, \varphi_{,i}\right) - \bar{f}_i u_i + \bar{q}\varphi\right] d\Omega \\ &\quad - \int_{S_t^e} \bar{t}_i \tilde{u}_i dS + \int_{S_\omega^e} \bar{\omega}\tilde{\varphi} dS \end{aligned} \tag{7}$$

However, as pointed out in the introduction, simple FEMs (including those in off-the-shelf commercial programs) involve extremely large time and resources for computation as well as mesh-generation if we want to model the microstructure with its embedded inclusions and voids. We propose to model composite piezoelectric materials using a new efficient tool named MPCG.

In order to develop MPCGs, we consider independently assumed complete functions u_i and φ in each subdomain (or grain) Ω^e, and introduce additional inter-grain compatible fields $\tilde{u}_i$ and $\tilde{\varphi}$ which satisfy displacement continuity and essential boundary conditions a-priori. Then we can derive the following hybrid variational principle, which is an extension of the pure mechanical model in Atluri [23]:

$$\begin{aligned} \pi\left(u_i, \varphi, \tilde{u}_i, \tilde{\varphi}\right) &= \sum_e \pi^e, \\ \pi^e &= \int_{\Omega^e} \left[H\left(u_{(i,j)}, \varphi_{,i}\right) - \bar{f}_i u_i + \bar{q}\varphi\right] d\Omega \\ &\quad - \int_{S_t^e} \bar{t}_i \tilde{u}_i + \int_{S_\omega^e} \bar{\omega}\tilde{\varphi} dS \\ &\quad - \int_{\partial\Omega^e} t_i\left(u_i - \tilde{u}_i\right) dS + \int_{\partial\Omega^e} \omega\left(\varphi - \tilde{\varphi}\right) dS \end{aligned} \tag{8}$$

where $t_j = n_i \frac{\partial H}{\partial u_{(i,j)}}$, $\omega = -n_i \frac{\partial H}{\partial \varphi_{,i}}$ and n_i is a unit vector normal to the grain boundary.

Now we consider that an inclusion or a void Ω_c^e is present inside each Ω^e, which satisfies $\Omega_c^e \subset \Omega^e$, $\partial\Omega_c^e \cap \partial\Omega^e = \emptyset$. We denote the matrix material as Ω_m^e, such that $\Omega_m^e = \Omega^e - \Omega_c^e$, $\partial\Omega_m^e = \partial\Omega^e + \partial\Omega_c^e$. Detailed illustration of the geometry can be found in Fig. 1 (left).

We use u_i^m, φ^m and u_i^c, φ^c to denote fields in Ω_m^e and Ω_c^e respectively. Linear inter-grain compatible fields $\tilde{u}_i^m$, $\tilde{\varphi}^m$ are assumed at the outer boundary $\partial\Omega^e$. Parabolic inter-element compatible fields $\tilde{u}_i^c$, $\tilde{\varphi}^c$ are assumed at the matrix-inclusion interface $\partial\Omega_c^e$ [(See Fig. 1 (right)]. If the grain contains a void instead of an inclusion, u_i^c, φ^c do not exist.

We deal with this configuration by constructing finite element equations for the inclusion material alone as a homogeneous (simply-connected) domain with nodes along the inclusion boundary as shown in Fig. 2 (right), and finite ele-

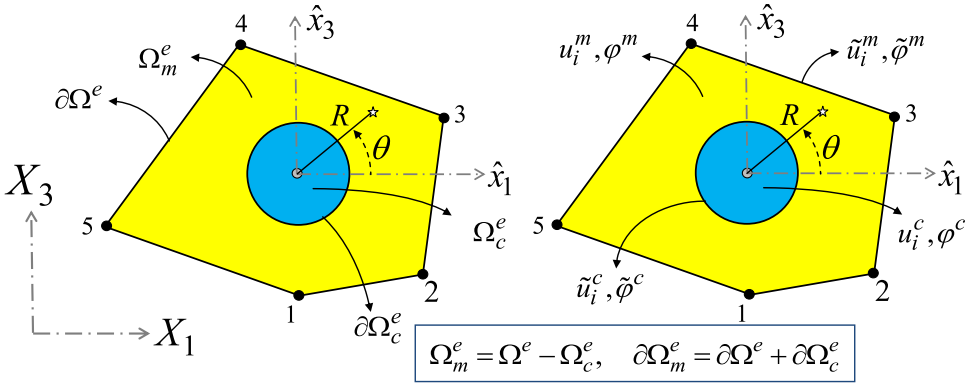

Fig. 1 A 2D MPCG containing an inclusion or a void (independent trial displacement fields are used)

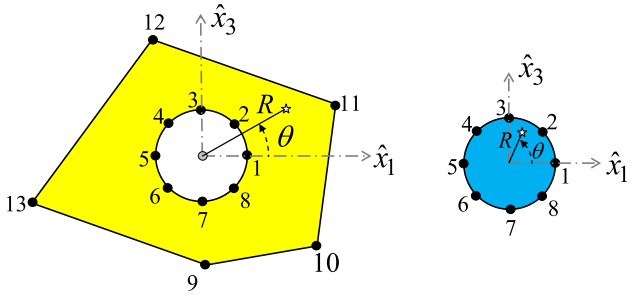

Fig. 2 MPCG matrix and inclusion domains, boundaries and boundary nodes

ment equations for the matrix material alone as a doubly-connected domain with nodes on both outer and inner boundaries [(Fig. 2 (left)]. Special trial functions are needed in dealing with the doubly-connected domain and are presented in the next section. Figure 2 shows an inclusion with eight boundary nodes which are also among the nodes of the matrix material together with the outer element (grain) nodes.

Assembling the matrix element and the inclusion element in the same way we assemble any two finite elements will assure the stress and electric displacement reciprocity as well as the continuity of the primal fields along the inclusion boundaries and results in an element (a grain) that describe the composite. If a grain contains a void instead of an inclusion, there is no need for this assembly.

3 Independent trial mechanical and electric fields, and the formulation of MPCG

It is clear that the boundary fields, $\tilde{u}_i^c, \tilde{\varphi}^c, \tilde{u}_i^m, \tilde{\varphi}^m$, should all be interpolated using node-based polynomial shape functions. On the other hand, the trial mechanical and electrical fields inside the matrix and inclusion materials, i.e. $u_i^m, \varphi^m, u_i^c, \varphi^c$, should be carefully selected. In the following discussion, we only focus on displacements because the electric potential trial functions are selected similarly.

We consider a 2D MPCG with an inclusion for example (see Fig. 1). Because the inclusion is a simply-connected domain, it is clear that the trial displacement field u_i^c can be represented as:

$$\begin{aligned} u_i^c &= f^c(R)\, g^c(\theta) \\ f^c(R) &= \alpha_0 + \alpha_1 R + \alpha_2 R^2 \ldots \\ g^c(\theta) &= \beta_0 + \beta_1 \cos\theta + \beta_2 \sin\theta + \beta_3 \cos 2\theta + \beta_4 \sin 2\theta \ldots \end{aligned} \tag{9}$$

where (R, θ) are the polar coordinates (see Figs. 1, 2). On the other hand, because the matrix material is a doubly connected domain, singular fields are included in the assumption of u_i^m:

$$\begin{aligned} u_i^m &= f^m(R)\, g^m(\theta) \\ f^m(R) &= \gamma_0 + \gamma_1 R + \gamma_2 R^2 \ldots + \gamma_{-1} R^{-1} + \gamma_{-2} R^{-2} \ldots \\ g^m(\theta) &= \lambda_0 + \lambda_1 \cos\theta + \lambda_2 \sin\theta + \lambda_3 \cos 2\theta + \lambda_4 \sin 2\theta \ldots \end{aligned} \tag{10}$$

It is obvious that for 3D problems, the displacement field should be assumed in a form of $u_i = f(R)\, g(\theta)\, h(\phi)$, where (R, θ, ϕ) are the spherical coordinates. The trial electric potential can be assumed in a similar fashion.

Using matrix and vector notation, we express the electromechanical displacements as:

$$\begin{aligned} \underline{\tilde{\mathbf{u}}}^m &= \begin{Bmatrix} \tilde{\mathbf{u}}^m \\ \tilde{\varphi}^m \end{Bmatrix} = \tilde{\mathbf{N}}_m \begin{Bmatrix} \mathbf{q} \\ \mathbf{q}_c \end{Bmatrix} = \tilde{\mathbf{N}}_m \mathbf{q}_m \ \text{ at } \partial\Omega_m^e \\ \underline{\mathbf{u}}^m &= \begin{Bmatrix} \mathbf{u}^m \\ \varphi^m \end{Bmatrix} = \mathbf{N}_m \boldsymbol{\alpha}_m \text{ in } \Omega_m^e \\ \underline{\tilde{\mathbf{u}}}^c &= \begin{Bmatrix} \tilde{\mathbf{u}}^c \\ \tilde{\varphi}^c \end{Bmatrix} = \tilde{\mathbf{N}}_c \mathbf{q}_c \ \text{ at } \partial\Omega_c^e \end{aligned} \tag{11}$$

and in case there is an inclusion, we also have:

$$\mathbf{u}^c = \begin{Bmatrix} \mathbf{u}^c \\ \varphi^c \end{Bmatrix} = \mathbf{N}_c \boldsymbol{\alpha}_c \text{ in } \Omega_c^e \tag{12}$$

where $\mathbf{q}$ and $\mathbf{q}_c$ are nodal electromechanical displacements on the outer and inner boundaries respectively, while $\boldsymbol{\alpha}_m$ and

$\boldsymbol{\alpha}_c$ are undetermined coefficients. $\tilde{\mathbf{N}}_m$ and $\tilde{\mathbf{N}}_c$ are shape functions (linear along the outer boundary and parabolic along the circular void/inclusion boundary), while $\mathbf{N}_m$ and $\mathbf{N}_c$ are functions extracted from Eqs. (10) and (9) respectively.

The secondary fields are derived from the primary fields and expressed as:

$$\underline{\boldsymbol{\varepsilon}}^m = \begin{Bmatrix} \boldsymbol{\varepsilon}^m \\ \mathbf{E}^m \end{Bmatrix} = \mathbf{B}_m \boldsymbol{\alpha}_m \text{ in } \Omega_m^e$$

$$\underline{\mathbf{t}}^m = \begin{Bmatrix} \mathbf{t}^m \\ \omega^m \end{Bmatrix} = \mathbf{n}\underline{\boldsymbol{\sigma}}^m = \mathbf{n}\underline{\mathbf{C}}_m\underline{\boldsymbol{\varepsilon}}^m = \mathbf{T}_m \boldsymbol{\alpha}_m \text{ at } \partial\Omega_m^e$$

$$\underline{\boldsymbol{\varepsilon}}^c = \begin{Bmatrix} \boldsymbol{\varepsilon}^c \\ \mathbf{E}^c \end{Bmatrix} = \mathbf{B}_c \boldsymbol{\alpha}_c \text{ in } \Omega_c^e$$

$$\underline{\mathbf{t}}^c = \begin{Bmatrix} \mathbf{t}^c \\ \omega^c \end{Bmatrix} = \mathbf{n}\underline{\boldsymbol{\sigma}}^c = \mathbf{n}\underline{\mathbf{C}}_c\underline{\boldsymbol{\varepsilon}}^c = \mathbf{T}_c \boldsymbol{\alpha}_c \text{ at } \partial\Omega_c^e \tag{13}$$

where $\underline{\mathbf{C}}_m$ and $\underline{\mathbf{C}}_c$ are the matrices of electromechanical material properties of the matrix and inclusion respectively, and

$$\mathbf{n} = \begin{bmatrix} n_x & 0 & n_y & 0 & 0 \\ 0 & n_y & n_x & 0 & 0 \\ 0 & 0 & 0 & n_x & n_y \end{bmatrix}$$

where $[n_x \;\; n_y]$ is the normal unit vector directed away from boundaries $\partial\Omega_m^e$ or $\partial\Omega_c^e$.

Substituting the trial solutions (11)–(13) into the hybrid variational principle (8) and ignoring the body force and the electric charge density, an FEM-type of equation can be developed for the inclusion as:

$$\pi_c^e(\boldsymbol{\alpha}_c, \mathbf{q}_c) = \boldsymbol{\alpha}_c^T \frac{1}{2}\mathbf{H}_c\boldsymbol{\alpha}_c - \boldsymbol{\alpha}_c^T\mathbf{P}_c\boldsymbol{\alpha}_c + \boldsymbol{\alpha}_c^T\mathbf{G}_c\mathbf{q}_c - \mathbf{q}_c^T\mathbf{f}_c \tag{14}$$

where

$$\mathbf{H}_c = \int_{\Omega_c^e} \mathbf{B}_c^T\underline{\mathbf{C}}_c\mathbf{B}_c d\Omega, \quad \mathbf{G}_c = \int_{\partial\Omega_c^e} \mathbf{T}_c^T\tilde{\mathbf{N}}_c dS,$$

$$\mathbf{P}_c = \int_{\partial\Omega_c^e} \mathbf{T}_c^T\mathbf{N}_c dS, \quad \mathbf{f}_c = \int_{S_t^e, S_\omega^e} \bar{\mathbf{t}}\tilde{\mathbf{N}}_c dS$$

Setting the variation of π_c^e to zero, we get the FEM equation as:

$$\delta\pi_c^e(\delta\boldsymbol{\alpha}_c, \delta\mathbf{q}_c) = \delta\boldsymbol{\alpha}_c^T\left[(\mathbf{H}_c - \mathbf{P}_c - \mathbf{P}_c^T)\alpha_c + \mathbf{G}_c\mathbf{q}_c\right] + \delta\mathbf{q}_c^T(\mathbf{G}_c^T\boldsymbol{\alpha}_c - \mathbf{f}_c) = 0 \tag{15}$$

and for arbitrary $\delta\boldsymbol{\alpha}_c^T$ and $\delta\mathbf{q}_c^T$, we get:

$$\boldsymbol{\alpha}_c = (\mathbf{P}_c + \mathbf{P}_c^T - \mathbf{H}_c)^{-1}\mathbf{G}_c\mathbf{q}_c = \mathbf{V}_c\mathbf{q}_c,$$
$$\mathbf{G}_c^T\boldsymbol{\alpha}_c = \mathbf{G}_c^T\mathbf{V}_c\mathbf{q}_c = \mathbf{K}_c\mathbf{q}_c = \mathbf{f}_c \tag{16}$$

Similarly for the matrix domain,

$$\boldsymbol{\alpha}_m = (\mathbf{P}_m + \mathbf{P}_m^T - \mathbf{H}_m)^{-1}\mathbf{G}_m\mathbf{q}_m = \mathbf{V}_m\mathbf{q}_m,$$
$$\mathbf{G}_m^T\boldsymbol{\alpha}_m = \mathbf{G}_m^T\mathbf{V}_m\mathbf{q}_m = \mathbf{K}_m\mathbf{q}_m = \mathbf{f}_m \tag{17}$$

where

$$\mathbf{H}_m = \int_{\Omega_m^e} \mathbf{B}_m^T\underline{\mathbf{C}}_m\mathbf{B}_m d\Omega, \quad \mathbf{G}_m = \int_{\partial\Omega_m^e} \mathbf{T}_m^T\tilde{\mathbf{N}}_m dS,$$

$$\mathbf{P}_m = \int_{\partial\Omega_m^e} \mathbf{T}_m^T\mathbf{N}_m dS, \quad \mathbf{f}_m = \int_{S_t^e, S_\omega^e} \bar{\mathbf{t}}\tilde{\mathbf{N}}_m dS.$$

Assembling the matrix and inclusion matrices, we get:

$$\begin{bmatrix} \mathbf{K}_{m1} & \mathbf{K}_{m2} \\ \mathbf{K}_{m2}^T & \mathbf{K}_{m3} + \mathbf{K}_c \end{bmatrix} \begin{Bmatrix} \mathbf{q} \\ \mathbf{q}_c \end{Bmatrix} = \begin{Bmatrix} \mathbf{f} \\ \mathbf{f}_c \end{Bmatrix} \tag{18}$$

Recognizing that $\mathbf{f}_c = \mathbf{0}$, $\mathbf{q}_c$ can be expressed in terms of $\mathbf{q}$ as:

$$\mathbf{q}_c = -(\mathbf{K}_{m3} + \mathbf{K}_c)^{-1}\mathbf{K}_{m2}^T\mathbf{q} = \mathbf{V}\mathbf{q} \tag{19}$$

Then we can write the final FEM equation in terms of the outer boundary nodal electromechanical displacements as:

$$(\mathbf{K}_{m1} + \mathbf{K}_{m2}\mathbf{V})\,\mathbf{q} = \mathbf{K}\mathbf{q} = \mathbf{f} \tag{20}$$

From the development of MPCGs, we can clearly see that the discretization of the domain requires minimal efforts since each MPCG can represent a physical grain of material (irregular polygon) with an inclusion or a void. For a typical RVE with a few hundred physical material grains, the meshing using MPCGs can take only few seconds. On the other hand, mesh generation using FEM takes enormous time, which makes the study of composite piezoelectric materials microstructures with conventional FEM very difficult or impossible.

4 Numerical examples

The formulation described above is programmed using MATLAB in a 64-bit WINDOWS operating system, and executed on a PC computer equipped with Intel Q8300 2.5GHz CPU, and 8GB RAM. The properties of the materials used in this section are listed in Table 1: PZT-4 from two references: Wang et al. [24] and Wang et al. [25] denoted PZT-4(1) and PZT-4(2) respectively, PVDF and SiC from [28].

Simple problems that use grains with no voids or inclusions, such as patch test and bending of a meso-scale piezoelectric panel, can be easily and accurately modeled using any number of grains (with no voids or inclusions) to mesh the problem domain, and the error in the whole structure is less than 1 %. Patch test with any number of grains containing inclusions having the same material properties as that of the matrix can also be passed with error less than 1 %.

In the following, we show some numerical examples using the proposed MPCGs. In the first two subsections we present a piezoelectric domain with an impermeable circular void

Table 1 Material properties used in the numerical examples

Property	PZT-4(1)	PZT-4(2)	PVDF	SiC particles
C_{11}(GPa)	139	126	3.8	483.7
C_{12}(GPa)	77.8	77.8	1.9	99.1
C_{13}(GPa)	74.3	74.3	1.0	99.1
C_{22}(GPa)	139	126	3.2	483.7
C_{23}(GPa)	74.3	74.3	0.9	99.1
C_{33}(GPa)	113	115	1.2	483.7
C_{44}(GPa)	25.3	25.6	0.7	192.3
C_{55}(GPa)	25.3	25.6	0.9	192.3
C_{66}(GPa)	30.6	30.6	0.9	192.3
e_{31}(C/m^2)	−6.98	−5.2	0.024	0.0
e_{32}(C/m^2)	−6.98	−5.2	0.001	0.0
e_{33}(C/m^2)	13.84	15.1	−0.027	0.0
e_{15}(C/m^2)	13.44	12.7	0.0	0.0
h_{11} (pC/(Vm)^2)	6	6.464	7.4	10.0
h_{22} (pC/(Vm)^2)	6	6.464	9.3	10.0
h_{33} (pC/(Vm)^2)	5.47	5.622	7.6	10.0

or inclusion under mechanical loading, followed by evaluation of material properties of porous piezoelectric material as functions of porosity volume fraction. Material properties of piezoelectric particulate composite (SiC particles in PVDF matrix) are also determined as functions of particle volume fraction in the last subsection. Comparisons with other analytical and computational results are presented whenever possible.

4.1 Infinite piezoelectric panel with an impermeable circular void

Consider an infinite piezoelectric plane with a circular void subjected to vertical mechanical loading in the far field. For numerical implementations, the infinite domain is truncated into a rectangle with length L and width W, as shown in Fig. 3. The global coordinate system is denoted $X_1 - X_3$ and the poling direction is aligned with the global vertical X_3 axis (shown in blue in the figure). The material is PZT-4(1) whose properties are presented in Table 1 and plane strain assumption is used in this problem. Here we take $L = W = 20a$, $\sigma_o = 1Pa$.

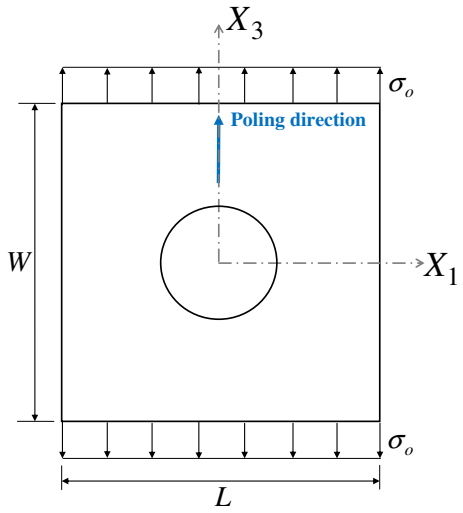

Fig. 3 A Finite rectangular domain with a circular void

The discrete extreme error defined in Eq. (21) is 0.0740.

$$E^e = \max_{\mathbf{x}_i \in \partial\Omega_c} \left(\frac{\left|\sigma_\theta(\mathbf{x}_i) - \tilde{\sigma}_\theta(\mathbf{x}_i)\right|}{\tilde{\sigma}_{\max}}, \frac{\left|D_\theta(\mathbf{x}_i) - \tilde{D}_\theta(\mathbf{x}_i)\right|}{\tilde{D}_{\max}} \right) \tag{21}$$

where $\tilde{\sigma}_\theta(\mathbf{x}_i)$ and $\tilde{D}_\theta(\mathbf{x}_i)$ are the exact solutions at boundary points $\mathbf{x}_i$ along the periphery of the void; $\tilde{\sigma}_{\max}$ and $\tilde{D}_{\max}$ are respectively the maximum magnitudes of $\tilde{\sigma}_\theta(\mathbf{x}_i)$ and $\tilde{D}_\theta(\mathbf{x}_i)$.

Figures 4 and 5 show the computed circumferential distributions of σ_θ, D_θ, E_θ and E_r divided by σ_o using one MPCG. Because of symmetry, the figures show the variables as θ goes from 0 to 90 degrees. The analytical solution [26]

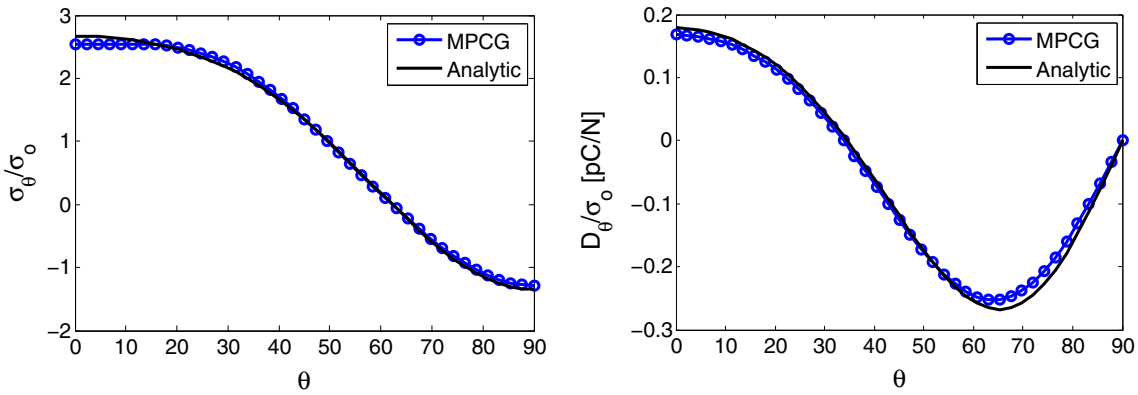

Fig. 4 Circumferential stress and electric displacement on the periphery of the void

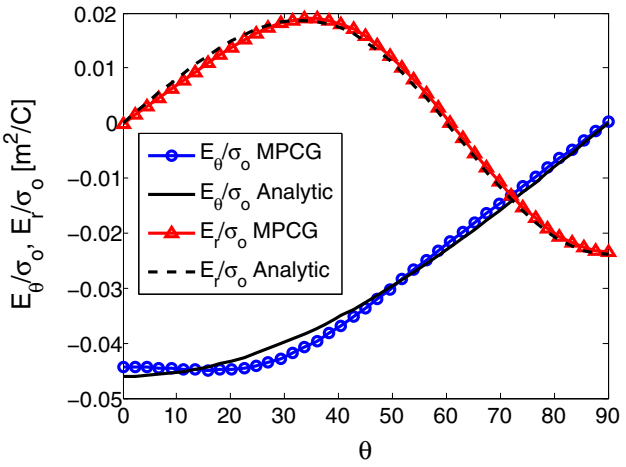

Fig. 5 Circumferential and radial components of electric field on the periphery of the void

is also included for comparison. Very good agreement can be seen.

4.2 Piezoelectric panel with circular inclusion

Now consider replacing the void in the previous example with an inclusion whose properties are given as: $\mathbf{C}_c = \mu\mathbf{C}_m$ where μ is a factor that can be varied. $\mu > 1$ is equivalent to an inclusion material with stronger properties than those of the matrix material (larger stiffness, dielectric and piezoelectric material constants), while $\mu < 1$ is equivalent to an inclusion with weaker properties. Figure 6 shows the effect of μ on σ_θ/σ_o, D_θ/σ_o, E_θ/σ_o and E_r/σ_o along the inclusion periphery.

It can be seen from the figure that the magnitude of the maximum circumferential stress, electric displacement and electric field along the inclusion periphery are significantly affected by the value of μ. Also the location of the maximum circumferential electric displacement and radial electric field are affected by the value of μ. As μ increases (stronger inclusion properties), the peak value of the circumferential stress is significantly decreased. Hence, we conclude that controlling the material properties of inclusions can result in preventing high stress concentrations around inclusions. Variables like μ can be used in optimal design of piezoelectric composite microstructures where stress concentrations around fibers and inclusions are taken into account. This was not considered in the optimal design of piezoelectric microstructures presented in many published research papers such as [27] for instance where topology optimization was used.

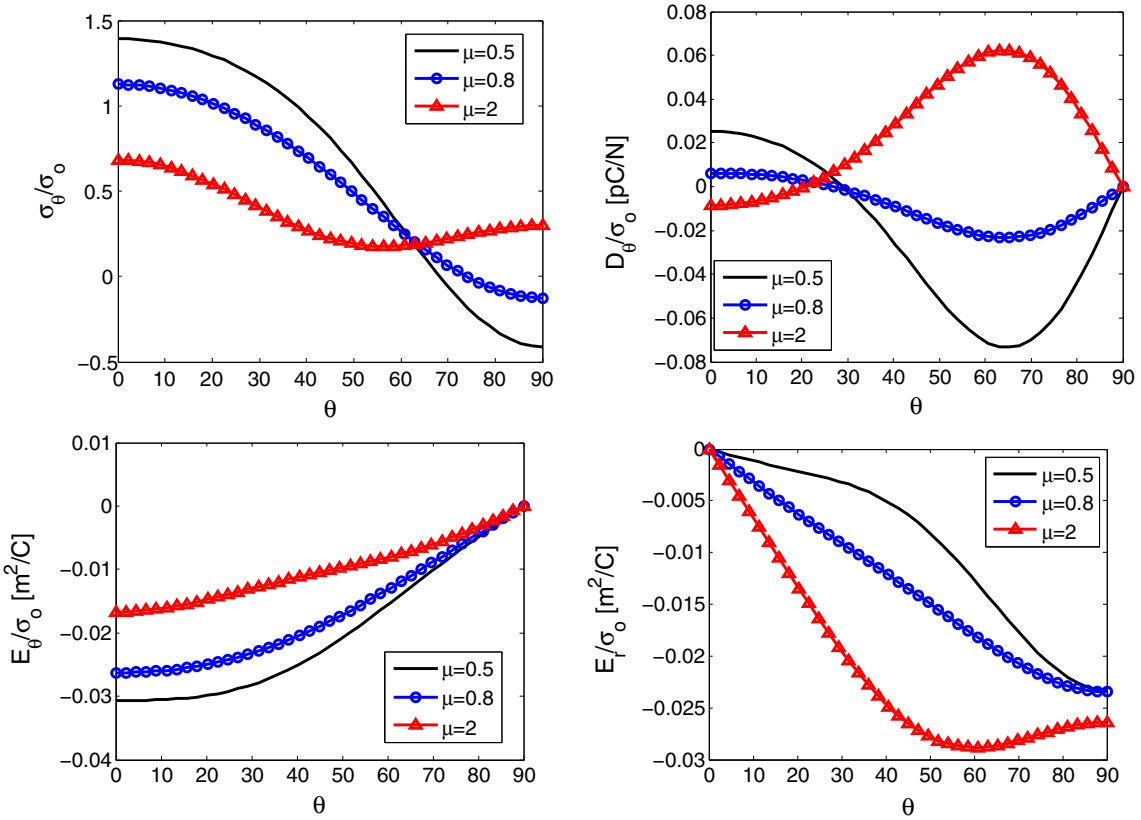

Fig. 6 The effect of μ on σ_θ/σ_o, D_θ/σ_o, E_θ/σ_o and E_r/σ_o along the inclusion periphery

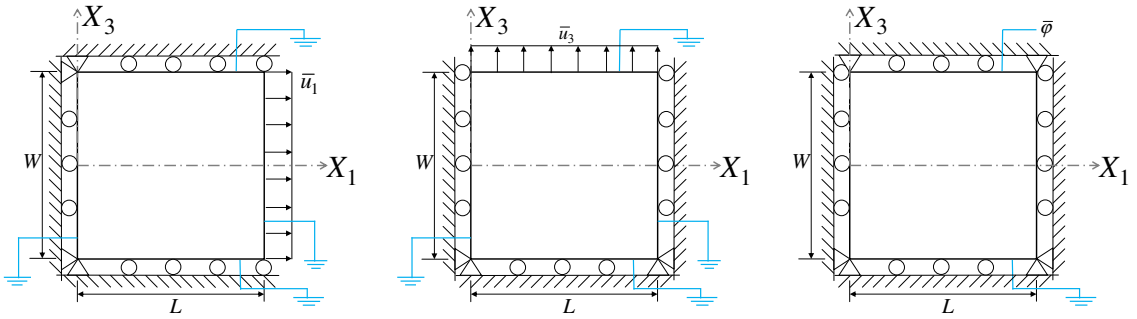

Fig. 7 Computational models to evaluate the effective properties of: (*left*) C_{11}^{eff} and C_{13}^{eff}, (*middle*) C_{33}^{eff} and C_{13}^{eff}, (*right*) e_{31}^{eff}, e_{33}^{eff} and h_{33}^{eff}

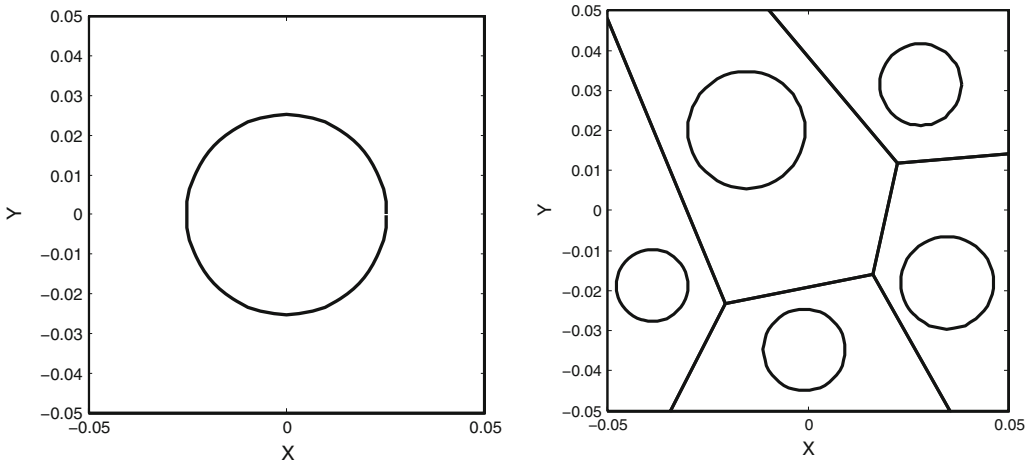

Fig. 8 Two representative volume elements (RVEs) used in the simulations

4.3 Evaluation of the effective material properties of porous piezoelectric materials

In this subsection, we determine the material properties of a porous PZT-4 ceramic sample as functions of porosity volume fraction using different MPCG samples. The material properties of non-porous PZT-4 are listed in Table 1 [(denoted PZT-4(2)]. Three computational models, shown in Fig. 7, are assumed to calculate the effective properties of the porous PZT-4: C_{11}^{eff}, C_{33}^{eff}, C_{13}^{eff}, e_{31}^{eff}, e_{33}^{eff} and h_{33}^{eff}.

The first model ensures that $\varepsilon_{33} = 0$ and $E_3 = 0$ and is used to calculate C_{11}^{eff} and C_{13}^{eff} as:

$$C_{11}^{eff} = \frac{\sigma_{11}}{\varepsilon_{11}} = \frac{\int_{x_1=L} t_1.ds/W}{\bar{u}_1/L},$$
$$C_{13}^{eff} = \frac{\sigma_{33}}{\varepsilon_{11}} = \frac{\int_{x_3=W/2} t_3.ds/L}{\bar{u}_1/L} \tag{22}$$

The second model ensures that $\varepsilon_{11} = 0$ and $E_3 = 0$ and is used to calculate C_{33}^{eff}, C_{13}^{eff} as:

$$C_{33}^{eff} = \frac{\sigma_{33}}{\varepsilon_{33}} = \frac{\int_{x_3=W/2} t_3.ds/L}{\bar{u}_3/W},$$
$$C_{13}^{eff} = \frac{\sigma_{11}}{\varepsilon_{33}} = \frac{\int_{x_1=L} t_1.ds/W}{\bar{u}_3/W} \tag{23}$$

Finally, the third model ensures that $\varepsilon_{11} = \varepsilon_{33} = 0$ and is used to calculate e_{33}^{eff}, e_{13}^{eff} and h_{33}^{eff} as:

$$e_{33}^{eff} = -\frac{\sigma_{33}}{E_3} = \frac{\int_{x_3=W/2} t_3.ds/L}{\bar{\varphi}/W},$$
$$e_{13}^{eff} = -\frac{\sigma_{11}}{E_3} = \frac{\int_{x_1=L} t_1.ds/W}{\bar{\varphi}/W},$$
$$h_{33}^{eff} = \frac{D_3}{E_3} = \frac{\int_{x_3=W/2} Q.ds/L}{\bar{\varphi}/W} \tag{24}$$

Two types of representative volume element (RVE) are used here as shown in Fig. 8 (the figure shows the case of VF=20 %): (a) a unit cell grain with a circular void, (b) five MPCG grains with random circular voids. A constraint was used in this mesh in order to prevent the radius of the void in any grain from exceeding 80% of the distance between the center of the void and the closest point to it on the grain's outer boundary. Plane strain assumption is used

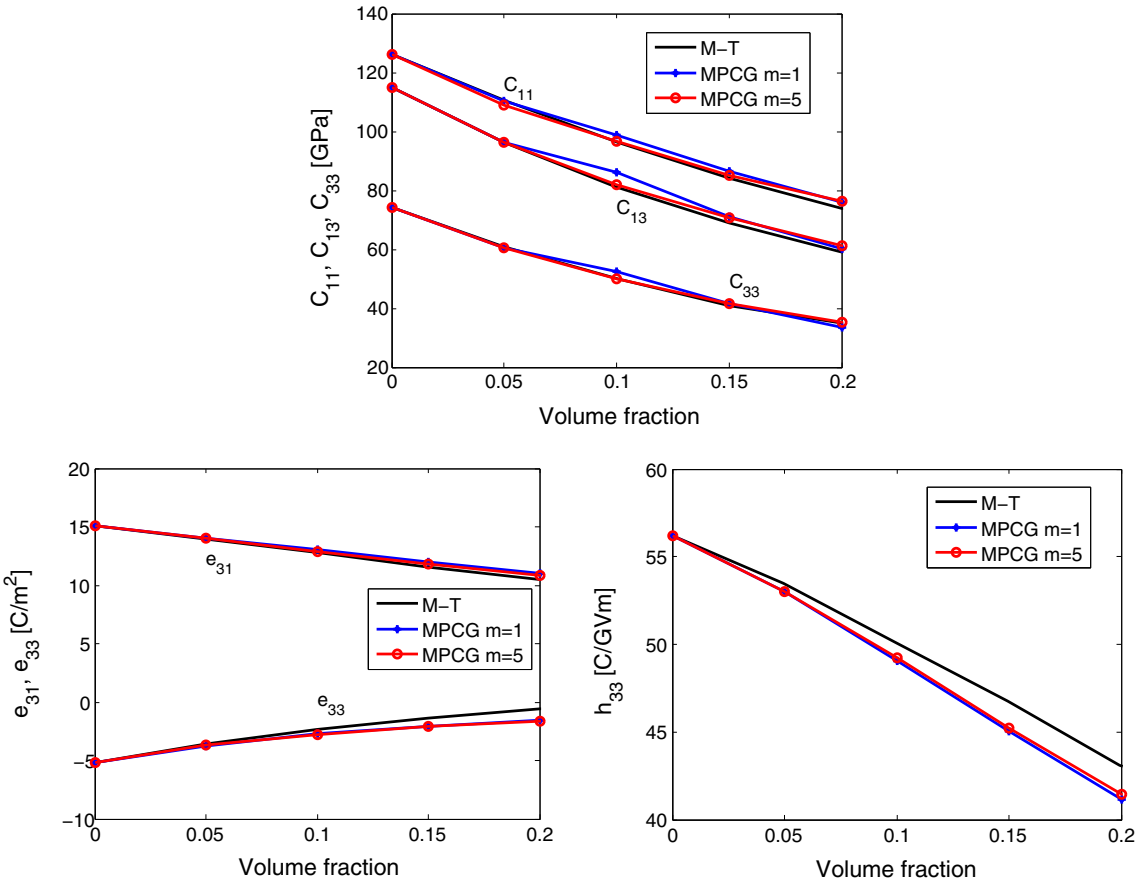

Fig. 9 Predictions of the effective piezoelectric material properties of PZT-4 as functions of porosity volume fraction (m is the number of grains used in the simulation)

in this study and the direction of polarization is assumed vertically upward in all grains. The results are compared with the predictions of Mori-Tanaka's model [4] presented in [25] for PZT-4.

Figure 9 shows the predictions of the effective properties of PZT-4 as functions of porosity volume fraction. The figure shows very good agreement with the predictions of Mori-Tanaka's analytical model.

It should be noted that, with the same number of grains, the results slightly change as the irregular mesh changes because the stiffness matrices depend on grain shapes. Increasing the number of grains and the number of nodes per side in each grain (i.e., using more than two nodes per side) generally has the effect of decreasing this effect.

4.4 Evaluation of the effective material properties of piezoelectric composite material

The effective properties of SiC/PVDF particulate composite is determined here and compared with other analytical and computational models. PVDF is an orthotropic, semi-crystalline polymer which exhibits piezoelectric effects if subjected to electric field along the X_3-axis. The PVDF polymer is reinforced with spherical SiC particles. Typical electromechanical properties of PVDF (supplied by NASA Langley Research Center) and SiC taken from [28] are given in Table 1. The numerical models used in the previous example are also used here to determine the effective material properties as functions of particle volume fraction. One MPCG grain polarized in the vertical direction is used in this simulation.

Since the particles are spherical, all effective material properties can be determined using 2D models. Considering the $x_1 - x_3$ plane, we can determine the properties: $C_{11}, C_{13}, C_{33}, e_{31}, e_{33}, h_{11}$, and h_{33}, considering the $x_2 - x_3$ plane, we can determine the properties: $C_{22}, C_{23}, C_{33}, e_{32}, e_{33}, h_{22}$, and h_{33}, while considering the $x_1 - x_2$ plane, only the properties: $C_{11}, C_{12}, C_{22}, h_{11}$, and h_{22} can be determined. Note that specifying the electric field in the horizontal direction, E_1, is equivalent to specifying $\bar{\varphi}$ on the right side of the model instead of the upper side [(see Fig. 7 (left)]. The three Young's moduli Y_1, Y_2, and Y_3 can be obtained from the stiffness matrix constants C_{ij}.

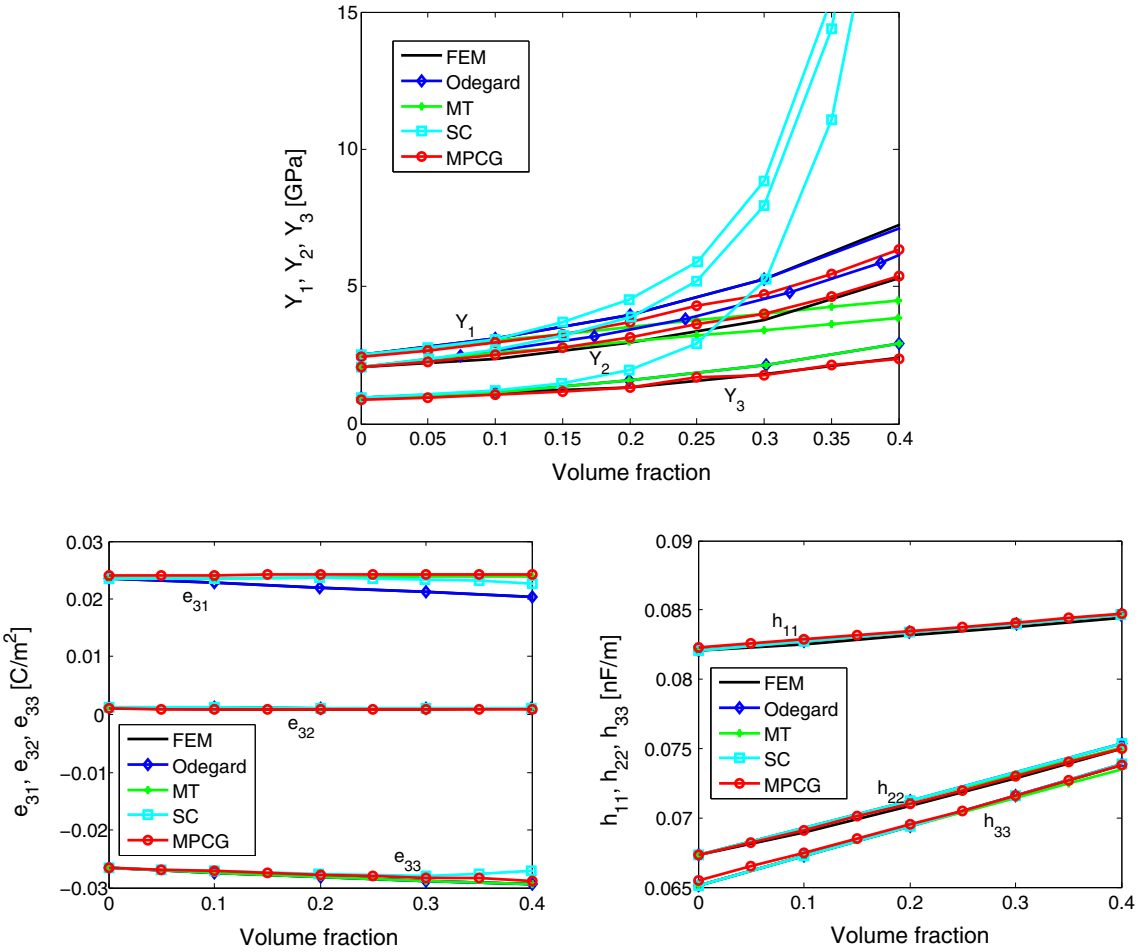

Fig. 10 Predictions of the effective properties of SiC/PVDF piezoelectric composite as functions of particle volume fraction

Figure 10 presents the predictions of the different effective material constants as functions of particle volume fraction and compared with Mori–Tanaka (MT), self consistent (SC), Finite Element models using ANSYS (with large number of elements) and Odegard's proposed models, all presented in [28].

It can be seen that, using only one MPCG grain, the proposed model gives very accurate predictions compared to Mori–Tanaka's analytical model. It is known that the self-consistent model deviates from Mori–Tanaka's model and gives unrealistic predictions as the volume fraction increases The proposed grains are much more computationally efficient as well as numerically more accurate, than the simple finite element models using ANSYS, and can be used to model piezo-composites even if the arrangement of particles is not symmetrical which is the main assumption used with all the previously mentioned analytical models.

5 Summary and conclusion

A new tool, which is not only mathematically highly accurate but also computationally very efficient, named MPCGs is proposed to study the micro-electro-mechanical behavior of composite piezoelectric materials. This method is based on a new hybrid variational principle, and independently assumed displacements and electric potentials in each MPCG. Each MPCG can efficiently model a single physical grain of the composite material, thus saving a significant time of generating a complex FEM meshes. MPCGs can also model porous and composite piezoelectric materials even if the distribution of voids/inclusions is not symmetrical (which is assumption used with all unit cell models). Because the trial solutions are complete but do not satisfy the governing differential equations a-priori, the formulation is very simple, and can account for local field concentrations efficiently and accurately. This was illustrated using different examples where the fields along the void/inclusion periphery were calculated, and the effective material properties of porous and composite materials were predicted, and compared with other analytical and computational models. The proposed MPCGs is expected to become a very powerful tool for direct numerical simulations (DNS) of the micro/meso mechanics of composite piezoelectric materials, and can possibly lead to efficient multi-scale modeling of piezoelectric devices. The extension

of the current MPCGs to nonlinear ferroelectric grains with embedded inclusions/voids to model the temporal evolution of the microscopic fields in ferroelectric composites will be pursued in our future study.

Acknowledgments This work was supported in part by the Vehicle Technology Division of the Army Research Labs, under a collaborative research agreement with University of California, Irvine (UCI). The encouragement of Dy Le and Jaret Riddick is thankfully acknowledged. Partial support of the DSR of King Abdulaziz University, Jeddah, is thankfully acknowledged.

References

1. Acmite Market Intelligence (2010) Market report: World piezoelectric device market
2. Bisegna P, Luciano R (1996) Variational bounds for the overall properties of piezoelectric composites. J Mech Phys Solids 44(4):583–602
3. Benveniste Y (1993) Universal relations in piezoelectric composites with eigenstress and polarization fields. I: binary media: local fields and effective behavior. J Appl Mech 60(2):265–269
4. Dunn ML, Taya M (1993) Micromechanics predictions of the effective electroelastic moduli of piezoelectric composites. Int J Solids Struct 30(2):161–175
5. Wang B (1992) Three-dimensional analysis of an ellipsoidal inclusion in a piezoelectric material. Int J Solids Struct 29(3):293–308
6. Chen T (1993) Piezoelectric properties of multiphase fibrous composites: some theoretical results. J Mech Phys Solids 41(11):1781–1794
7. Gaudenzi P (1997) On the electromechanical response of active composite materials with piezoelectric inclusions. Comput Struct 65(2):157–168
8. Poizat C, Sester M (1999) Effective properties of composites with embedded piezoelectric fibers. Comput Mater Sci 16(1–4):89–97
9. Li Z, Wang C, Chen C (2003) Effective electromechanical properties of transversely isotropic piezoelectric ceramics with microvoids. Comput Mater Sci 27(3):381–392
10. Berger H, Gabbert U, Koppe H, Rodriguez-Ramos R, Bravo-Castillero J, Guinovart-Diaz R, Otero JA, Maugin GA (2003) Finite element and asymptotic homogenization methods applied to smart composite materials. Comput Mech 33:61–67
11. Berger H, Kari S, Gabbert U, Rodriguez-Ramos R, Guinovart R, Otero JA, Bravo-Castillero J (2005) An analytical and numerical approach for calculating effective material coefficients of piezoelectric fiber composites. Int J Solids Struct 42(21):5692–5714
12. Kim JS, Arronche L, Farrugia A, Muliana A, La Saponara V (2011) Multi-scale modeling of time-dependent response of smart sandwich constructions. Compos Struct 93(9):2196–2207
13. Cook AC, Vel SS (2012) Multiscale analysis of laminated plates with integrated piezoelectric fiber composite actuators. Compos Struct 94(2):322–336
14. Keip M-A, Schröder J (2011) Effective electromechanical properties of heterogeneous piezoelectrics. In: Markert B (ed) Advances in extended and multifield theories for continua of lecture notes in applied and computational mechanics, vol 59. Springer, Berlin, pp 109–128
15. Schröder J, Keip M-A (2012) Two-scale homogenization of electromechanically coupled boundary value problems. Comput Mech 50:229–244
16. Dong L, Atluri SN (2012a) T-Trefftz Voronoi cell finite elements with eastic/rigid inclusions or voids for micromechanical analysis of composite and porous materials. CMES 83(2):183–219
17. Dong L, Atluri SN (2012b) Development of 3D T-Trefftz Voronoi cell finite elements with/without spherical voids & /or elastic/rigid inclusions for micromechanical modeling of heterogeneous materials. CMC 29(2):169–212
18. Dong L, Atluri SN (2012c) Development of 3D Trefftz Voronoi cells with ellipsoidal voids &/or elastic/rigid inclusions for micromechanical modeling of heterogeneous materials. CMC 30(1): 39–82
19. Bishay PL, Atluri SN (2014a) Trefftz-Lekhnitski Grains (TLGs) for efficient direct numerical simulation (DNS) of the micro/meso mechanics of porous piezoelectric materials. Comput Mater Sci 83:235–249
20. Bishay PL, Alotaibi A, Atluri SN (2014b) Multi-region Trefftz Collocation Grains (MTCGs) for modeling piezoelectric composites and porous materials in direct and inverse problems. J Mech Mater Struct 9(3)
21. Ding HJ, Liang J, Chen B (1996) Fundamental solution for transversely isotropic piezoelectric media. Sci China (A) 39:766–775
22. Bishay PL, Atluri SN (2013) 2D and 3D multiphysics Voronoi cells, based on radial basis functions, for Direct Mesoscale Numerical Simulation (DMNS) of the switching phenomena in ferroelectric polycrystalline materials. CMC 33(1):19–62
23. Atluri SN (1975) On hybrid finite element models in solid mechanics. In: Vichnevetsky R (ed) Advances in computer methods for partial differential equations. AICA, New Brunswick, pp 346–356
24. Wang XW, Zhou Y, Zhou WL (2004) A novel hybrid finite element with a hole for analysis of plane piezoelectric medium with defects. Int J Solids Struct 41:7111–7128
25. Wang H, Tan G, Cen S, Yao Z (2005) Numerical determination of effective properties of voided piezoelectric materials using BNM. Eng Anal Bound Elem 29:636–646
26. Sosa H (1991) Plane problems in piezoelectric media with defects. Int J Solids Struct 28(4):491–505
27. Nelli Silva EC, Ono Fonseca JS (1997) Optimal design of piezoelectric microstructures. Comput Mech 19:397–410
28. Odegard GM (2004) Constitutive modeling of piezoelectric polymer composites. Acta Mater 52:5315–5330